Journal of Natural Sciences and Mathematics
Qassim University, Vol. 11, No. 1, pp 15-28 (January 2018/Rabi II 1439H.)

Structural, magnetic and magnetocaloric properties of nickel-copper ferrite with chromium substitution

Abdulrahman Mallah

Qassim University, College of Science,

Department of Chemistry, Buraydah Almolaydah Buraydah

٥١٤٥٢P.O.Box: 6644, Saudi Arabia.

E-mail: a.mallah@qu.edu.sa

Abstract. The structural, magnetic and magnetocaloric properties of $Ni_{0.6}Cu_{0.4}Fe_{1.5}Cr_{0.5}O_4$ sample have been investigated. The sample was synthesized by sol-gel method. The X-ray diffraction result indicates that the ferrite sample has a cubic spinel type structure ($Fd\bar{3}m$ space group). Magnetization versus temperature showed that sample exhibits a second-order paramagnetic (PM) -ferromagnetic (FM) phase transitions with Curie temperature T_C equal to 660 K. Magnetocaloric properties were obtained by measuring a family of *M(H, T)* curves near T_C and calculating both magnetic entropy change (ΔS_M) and relative cooling power (RCP). The magnetic entropy change reaches a maximum value $|\Delta S_M^{max}|$ of about 1.39 $J.K^{-1}.kg^{-1}$ for $\mu_0 H$= 5 T corresponding to relative cooling power (RCP) of 142 $J.kg^{-1}$. These values are comparable to that of some other ferrite materials considered as possible candidates for magnetic refrigeration.

Keywords: Ferrites; Sol-gel method; Magnetization; Second order transition; Magnetocaloric effect.

1. Introduction

Magnetic refrigeration is a promising technology to replace the conventional gas-compression refrigeration due to its high efficiency, small volume, energy saving and ecological cleanliness **[1]**. Magnetic refrigeration is based on the basic phenomenon known as the magnetocaloric effect (MCE) **[1]**. The MCE in terms of isothermal magnetic entropy change can be calculated either by using the adiabatic change of temperature under the application of a magnetic field or through the measurement of the initial isothermal magnetization as a function of the magnetic field at various temperatures.

Many materials have been fabricated and studied for magnetic refrigeration applications including Heusler alloys **[2-4]**, perovskite manganites **[5-7]**, and spinel ferrites **[8-15]**. Among these, spinel ferrite materials with the general molecular formula MFe_2O_4 (where M^{2+}= Mn^{2+}, Fe^{2+}, Co^{2+}, Ni^{2+}, Cu^{2+}, Zn^{2+}, etc.) have attracted much interest due to their possibility to be considered as possible candidates for magnetic refrigeration.

Among spinel ferrites, Ni–Cu ferrites are among the most important ferrites, which find a number of applications in sensors, magnetic technologies and in EMI shielding **[16, 17]**. The various compositions of $Ni_{1-x}Cu_xFe_2O_4$ system have been widely investigated and reported in literature **[18-21]**. Therefore, several substitutions with different metal ions such as Al, Co, Zn and Mg were made on Ni-Cu ferrite system in order to improve its practical applications **[22-25]**. However, the reports on magnetocaloric properties of Ni-Cu ferrites with Cr substitution are not reported in previous studies. In the present study, ferrite having composition $Ni_{0.6}Cu_{0.4}Fe_{1.5}Cr_{0.5}O_4$ was investigated. The sol-gel method was used to synthesize this sample. Firstly, the detailed synthesis process of the sample was presented. Then, the structural, magnetic and magnetocaloric properties of $Ni_{0.6}Cu_{0.4}Fe_{1.5}Cr_{0.5}O_4$ sample have been studied systematically.

2. Experimental

2.1. Preparation

$Ni_{0.6}Cu_{0.4}Fe_{1.5}Cr_{0.5}O_4$ sample was prepared by sol-gel method using stoichiometric amounts of $Ni(NO_3)_2.6H_2O$,$Cu(NO_3)_2.3H_2O$, $Fe(NO_3)_3.9H_2O$ and $Cr(NO_3)_3.9H_2O$ precursors (all chemicals were of 99.99% purity and purchased from Sigma Aldrich). Stoichiometric amounts of metal nitrates were first dissolved in distilled water to obtain a mixed solution. Subsequently, when these nitrates were completely dissolved in the solution, controlled amounts of citric acid were incorporated and dissolved with stirring. The molar ratio was fixed as 1:1 of nitrates to citric acid and pH of the solution was adjusted by adding an amount of ammonia.

Then the solution was heated under regular stirring to 373 K followed by the addition of ethylene glycol as a polymerization agent. Heating and stirring continued until obtaining a gel after about 4 h. The obtained gel was dried at 573 K to obtain a foamy dry which was ground in a mortar, followed by drying at 773 K for 12 h in air. The powder was pressed into pellets with diameter of 10 mm and thickness of about 2 mm and then sintered at 973 K for 24 h. After grinding, the pellets were pressed again, and then heating at 1173 K for 24 h. In order to obtain the desired crystalline phase, the obtained pellets undergo a third cycle of grinding and re-pelleting and finally sintered at 1473 K during a sufficiently long annealing period (48 h). Then, all the results found in the present investigation are presented for $Ni_{0.6}Cu_{0.4}Fe_{1.5}Cr_{0.5}O_4$ sample sintered at 1473 K. The detailed synthesis process of the sample is represented in Fig. 1.

2.2. Characterization

Powder X-ray diffraction (XRD) data were collected in the 2θ range 20°-70° with a step size of 0.017° and a counting time of 18 s per step using a "PANalytical X'Pert Pro" diffractometer with filtered (Ni filter) CuKα_1 radiation (λ = 1.5406 Å). Standard *Si* powder was used to obtain the instrumental resolution function. Morphology of the sample was analysed using scanning electron microscopy (SEM; Philips XL30 microscope) under an accelerating voltage of 15 kV. Magnetization as a function of the temperature *M(T)* and isothermal *M(H, T)* were performed using extraction magnetometer. The temperature dependence of the magnetization, *M(T)*, was measured in field cooled (FC) regime from room temperature to 750 K under a constant magnetic field ($\mu_0 H$= 0.1 T). Isothermal *M(H, T)* data were measured for different temperature ranges around the Curie temperature (T_C) by a step of 5 K under an applied magnetic field varying from 0 to 1 T by step of 0.1 T and from 1 to 5 T by step of 0.5 T.

3. Results and discussions

3.1. Structural analysis

Fig. 2 presents the X-ray diffraction patterns for $Ni_{0.6}Cu_{0.4}Fe_{1.5}Cr_{0.5}O_4$ sample. This figure indicates that the sample exhibits a single phase without any detectable of secondary phase. There are almost no diffraction peaks corresponding to impurity phases, suggesting that pure phase was obtained. Using "*X'Pert HighScore Plus*" software, the diffraction peaks are indexed with respect to the cubic spinel type structure (space group $Fd\bar{3}m$). The lattice constant was calculated from the XRD data using the following equation **[9]**:

$$\boldsymbol{a = \frac{\lambda}{2}\frac{\sqrt{h^2 + l^2 + k^2}}{sin\theta}} \quad (\mathbf{1})$$

where λ is the wavelength, a the lattice constant and $(h\ k\ l)$ are the corresponding Miller indices. The obtained lattice constant is a= 8.2986 Å that gives a cell volume of V= 581.498 Å^3. The X-ray density for $Ni_{0.6}Cu_{0.4}Fe_{1.5}Cr_{0.5}O_4$ sample was calculated according to the equation **[9]**:

$$\boldsymbol{\rho_x = \frac{8M}{Na^3}} \qquad (\mathbf{2})$$

where 8 represents the number of molecules in a unit cell of spinel lattice, M is the molecular weight of the sample, a is the lattice constant of the ferrite and N is Avogadro's number. The X-ray density of the sample is equal to 5.275 g/cm^3.

The obtained values of lattice constant (a) and X-ray density (ρ_x) for $Ni_{0.6}Cu_{0.4}Fe_{1.5}Cr_{0.5}O_4$ sample are lower than those obtained for the parent $Ni_{0.6}Cu_{0.4}Fe_2O_4$ sample **[26-28]**. On the one hand, the decrease in lattice constant may be attributed to the smaller ionic radius of Cr^{3+} (0.63 Å) compared with that of Fe^{3+} (0.645 Å) **[29]**. On the other hand, the low value of X-ray density compared with those obtained for $Ni_{0.6}Cu_{0.4}Fe_2O_4$ sample in Ref. **[27, 28]** can be due to the lower density of chromium (7.15 g/cm^3) compared with that of iron (7.87 g/cm^3).

From the most intense peak (3 1 1) shown in the left inset of Fig. 2, the average grain size of the synthesized material was calculated using the Debye–Scherer's equation **[17]**:

$$\boldsymbol{D = \frac{0.9\lambda}{\beta \cos(\theta)}} \qquad (\mathbf{3})$$

where, β is full width at half maxima (FWHM) (rad), λ is wavelength of X-rays (λ=1.5406 Å) and θ is diffraction angle. The estimated value of the average grain size of the sample is equal to 78 nm. The SEM micrograph (given in the right inset of Fig. 2) for $Ni_{0.6}Cu_{0.4}Fe_{1.5}Cr_{0.5}O_4$ sample shows unique chemical contrast corresponding to the ferrite phase and uniform grain size distribution with negligible porosity. The average grain size[1] obtained from SEM image is about 0.42 μm. This value is higher than that calculated from XRD data. This difference is due to the fact that observations by imaging techniques such as SEM often give the size of the secondary particles (collection of grains), and the X-ray line broadening analysis disclosed the size of primary particles (collection of crystallites) **[31]**.

[1] The average grain size may be estimated from SEM image using an intercept method, described as follows **[30]**: straight lines all the same lengths are drawn through several micrographs that show the grain structure. The grains intersected by each line segment are counted; the line length is then divided by an average of the number of grains intersected, taken over all the line segments. The average grain size is found by dividing this result by the linear magnification of the micrographs.

3.2. Magnetic and magnetocaloric properties

Magnetization measurements as a function of temperature at applied magneticfield of 0.1 T showed that the synthesized $Ni_{0.6}Cu_{0.4}Fe_{1.5}Cr_{0.5}O_4$ sample exhibits a ferromagnetic to paramagnetic (FM–PM) phase transition with increasing temperature (Fig. 3). The Curie temperature T_C can be obtained from the minimum value of *dM/dT* vs. *T* curve, as shown in the inset of Fig. 3. The obtained T_C value is found to be 660 K. This value is lower than that found by *H.V. Kiran* for $Ni_{0.6}Cu_{0.4}Fe_2O_4$ sample (T_C= 805 K) **[32]**. It is observed that the Curie temperature decreases with the substitution of magnetic Cr^{3+} ion less magnetic than Fe^{3+} ion.

Fig. 4 shows the isothermal magnetization $M(\mu_0 H, T)$ magnetic field dependency, measured for different temperatures near T_C= 660 K in the magnetic field range of 0-5 T for $Ni_{0.6}Cu_{0.4}Fe_{1.5}Cr_{0.5}O_4$ sample. The isothermal magnetization $M(\mu_0 H, T)$ measured at different temperatures below T_C, show a non linear behavior with a sharp increase for low field values and a tendency to saturation as field increases reflecting a ferromagnetic behavior. However for $T > T_C$, a drastically decrease of $M(H, T)$ is observed with an almost linear behavior reflecting a paramagnetic behavior, due to the thermal agitation which disrupts the arrangement of the magnetic moments.

In order, to determine the nature of the magnetic phase transition (first or second order) for $Ni_{0.6}Cu_{0.4}Fe_{1.5}Cr_{0.5}O_4$ sample, the Arrott diagram ($\mu_0 H/M$ *vs.* M^2) was presented in Fig. 5 **[33]**. From Fig. 5, the ($\mu_0 H/M$ *vs.* M^2) curves exhibit, in the vicinity of T_C, a positive slope that corresponds to the second-order phase transition, according to Banerjee's criterion **[34]**.

On the basis of the thermodynamical theory, the magnetic entropy change, ΔS_M, associated with magnetic field (H) variation is given by **[1]**:

$$\Delta \boldsymbol{S_M}(\boldsymbol{T}, \boldsymbol{\Delta H}) = \boldsymbol{S_M}(\boldsymbol{T}, \boldsymbol{H}) - \boldsymbol{S_M}(\boldsymbol{T}, \boldsymbol{0}) = \int_0^H \left(\frac{\partial \boldsymbol{M}}{\partial \boldsymbol{T}}\right)_H \boldsymbol{dH} \qquad (4)$$

For magnetization measured at discrete field and temperature intervals, the magnetic entropy change, ΔS_M is approximated as:

$$\Delta \boldsymbol{S_M}(\boldsymbol{T}, \boldsymbol{\Delta H}) = \sum \frac{\boldsymbol{M_i} - \boldsymbol{M_{i+1}}}{\boldsymbol{T_i} - \boldsymbol{T_{i+1}}} \boldsymbol{\Delta H_i} \qquad (5)$$

where M_i and M_{i+1} are the experimental values of the magnetization at T_i and T_{i+1}, respectively, under a magnetic field H_i. The magnetic entropy change is evaluated through the measurements shown in Fig. 4 of isothermal magnetization vs. magnetic field at various temperatures. For magnetization measured at discrete field and temperature intervals, the magnetic entropy change was calculated by using Eq.

(5). Fig. 6 shows the temperature dependences of $\Delta S_M(T,H)$ for $Ni_{0.6}Cu_{0.4}Fe_{1.5}Cr_{0.5}O_4$ sample at various magnetic fields. As seen from Fig. 5, the ΔS_M exhibits a maximum, $|\Delta S_M^{max}|$, near T_C= 660 K. This maximum increases with the increase of magnetic field which indicates that a larger entropy change is expected at higher magnetic field (1.39 $J.kg^{-1}K^{-1}$ for $\mu_0 H$ = 5T).

The order nature of the magnetic phase transition for $Ni_{0.6}Cu_{0.4}Fe_{1.5}Cr_{0.5}O_4$ sample can be also confirmed by using the universal behavior proposed by Franco et al. **[35]**. They proposed that the $\Delta S_M(T)$ curves measured with different maximum applied fields should collapse on to a single master curve for alloys with second order phase transition. The universal curve is made by using the normalized entropy change ($\Delta S_M/\Delta S_M^{max}$) as a function of the rescaled temperature (θ). The temperature axis can be rescaled in a different way below and above T_C, just by imposing that the position of two additional reference points in the curve correspond to $\theta = \pm 1$.

$$\boldsymbol{\theta} = \begin{cases} -(\boldsymbol{T}-\boldsymbol{T_C})/(\boldsymbol{T_{r1}}-\boldsymbol{T_C}), & \boldsymbol{T} \le \boldsymbol{T_C} \\ (\boldsymbol{T}-\boldsymbol{T_C})/(\boldsymbol{T_{r2}}-\boldsymbol{T_C}), & \boldsymbol{T} \ge \boldsymbol{T_C} \end{cases} \quad (\mathbf{6})$$

where T_{r1} and T_{r2} are the temperatures of the two reference points that have been selected as those corresponding to $0.5\,\Delta S_M^{max}$. It is clear from Fig. 7 that all normalized entropy change curves collapse into a single curve, which confirms the second order natureof the magnetic phase transition for $Ni_{0.6}Cu_{0.4}Fe_{1.5}Cr_{0.5}O_4$ sample.

The most meaningful parameter that provides a measure of the effectiveness of magnetic materials for applications in magnetic refrigeration is the relative cooling power (*RCP*) **[1]**. The *RCP* values at various magnetic fields were calculated using the following relation **[1]**:

$$\boldsymbol{RCP} = |\boldsymbol{\Delta S_M^{max}}| \times \boldsymbol{\delta T_{FWHM}} \quad (\mathbf{7})$$

where δT_{FWHM} is the fullwidth at half maximum of the magnetic entropy change curve. The $|\Delta S_M^{max}|$ and RCP values obtained for $Ni_{0.6}Cu_{0.4}Fe_{1.5}Cr_{0.5}O_4$ sample exhibit an almost linear rise with increasing the magnetic field as exemplified in Fig.8. In table 1, the performances of magnetocaloric effect corresponding to a magnetic field of 5 T for $Ni_{0.6}Cu_{0.4}Fe_{1.5}Cr_{0.5}O_4$ sample was compared with those of some others ferrite systems reported in the literature **[8, 10]**. As can be seen from table 1, the values of $|\Delta S_M^{max}|$ and *RCP* of $Ni_{0.6}Cu_{0.4}Fe_{1.5}Cr_{0.5}O_4$ sample is comparable to that of some other ferrite materials considered as possible candidates for magnetic refrigeration **[8, 10]**.

4. Conclusion

In summary, the structural, magnetic and magnetocaloric properties of $Ni_{0.6}Cu_{0.4}Fe_{1.5}Cr_{0.5}O_4$ sample were investigated. The sample crystallizes in the cubic spinel structure ($Fd\bar{3}m$ space group). Magnetic measurements show that the sample presents a second order FM - PM phase transition. The magnetic entropy change reached a maximum of 1.39 $J.K^{-1}.kg^{-1}$ for $\mu_0 H$= 5 T, corresponding to the RCP value of 142 $J.Kg^{-1}$. In order to confirm the nature of the PM–FM phase transition, a master curve behavior for the temperature dependence of ΔS_M measured for different maximum fields is proposed.

Acknowledgment

The author would like to extend his sincere appreciation to Central Lab in College of Science at Qassim University for support this work. The author expresses his sincere thanks to Dr. Sobhi Hcini for his keen interest and kind help throughout this work.

References

[1] Phan MH, Yu SC, Review of the magnetocaloric effect in manganite materials. J Magn Magn Mater. 2007; 308 (2): 325–340.

[2] Pecharsky VK, Gschneidner KA. Effect of alloying on the giant magnetocaloric effect of $Gd_5(Si_2Ge_2)$. J Magn Magn Mater. 1997; 167 (3): L179–L184.

[3] Wada H, Tanabe Y. Giant magnetocaloric effect of $MnAs_{1-x}Sb_x$. Appl Phys Lett. 2001; 79 (20): 3302–3304.

[4] Hu FX, Shen BG, Sun JR, et al. Influence of negative lattice expansion and metamagnetic transition on magnetic entropy change in the compound LaFe11.4Si1.6. Appl Phys Lett. 2001; 78: 3675–3677.

[5] Hcini S, Boudard M, Zemni S, et al. Effect of Fe-doping on structural, magnetic and magnetocaloric properties of $Nd_{0.67}Ba_{0.33}Mn_{1-x}Fe_xO_3$ manganites; Ceram Int. 2014: 40: 16041–16050.

[6] Oumezzine E, Hcini S, Hlil EK, et al. Effect of Ni-doping on structural, magnetic and magnetocaloric properties of $La_{0.6}Pr_{0.1}Ba_{0.3}Mn_{1-x}Ni_xO_3$ nanocrystalline manganites synthesized by Pechini sol–gel method. J Alloys Compd. 2014; 615: 553–560.

[7] Baazaoui M, Boudard M, Zemni S. Magnetocaloric properties in $Ln_{0.67}Ba_{0.33}Mn_{1-x}Fe_xO_3$ (Ln=La or Pr) manganites. Mater Lett. 2011; 65: 2093–2095.

[8] Oumezzine E, Hcini S, Baazaoui M, et al. Structural, magnetic and magnetocaloric properties of $Zn_{0.6-x}Ni_xCu_{0.4}Fe_2O_4$ ferrite nanoparticles prepared by Pechini sol-gel method. Powder Technol. 2015; 278:189–195.

[9] Anwar MS, Ahmed F, Koo BH. Enhanced relative cooling power of $Ni_{1-x}Zn_xFe_2O_4$ ($0.0 \leq x \leq 0.7$) ferrites. Acta Mater. 2014; 71: 100–107.

[10] Akhter S, Paul DP, Hoque SM, et al. Magnetic and magnetocaloric properties of $Cu_{1-x}Zn_xFe_2O_4$ (x=0.6, 0.7, 0.8) ferrites. J Magn Magn Mater. 2014; 367: 75–80.

[11] Chau N, Thuan NK, Minh DL, et al. Effects of Zn content on the magnetic and magnetocaloric properties of Ni-Zn ferrite. VNU J Sci Math Phys. 2008; 24: 155–162.

[12] Poddar P, Gass J, Rebar DJ, et al. Magnetocaloric effect in ferrite nanoparticles. J Magn Magn Mater. 2006; 307: 227–231.

[13] Mamiya H, Terada N, Furubayashi T, et al. Influence of random substitution on magnetocaloric effect in a spinel ferrite. J Magn Magn Mater. 2010; 322: 1561–1564.

[14] Lee KD, Kambale RC, Hur N. Magnetocaloric effect in Ni-Zn ferrite nanoparticles prepared by using solution combustion. J Korean Phys Soc. 2014; 65: 1930–1934.

[15] Tawfik A, Hemeda OM, Hemeda DM, et al. Structural and magnetocaloric properties of nano Zn ferrite doped with Ni under hydrothermal conditions. Eur Phys J Plus. 2014; 129: 278–290.

[16] Wang H, Zhu D, Zhou W, et al. Synthesis and microwave absorbing properties of Ni–Cu ferrite/MWCNTs composites. J Mater Sci: Mater Electron. 2015; 26: 7698–7704.

[17] Madhu BJ, Ashwini ST, Shruthi B, et al. Structural, dielectric and electromagnetic shielding properties of Ni–Cu nanoferrite/PVP composites. Mater Sci Eng B. 2014; 186: 1–6.

[18] Ahmed MA, Mansour SF, Afif M. Structural and electrical properties of nanometric Ni–Cu ferrites synthesized by citrate precursor method. J Magn Magn Mater. 2012; 324: 4–10.

[19] Gabal MA, Al Angari YM, Kadi MW. Structural and magnetic properties of nanocrystalline $Ni_{1-x}Cu_xFe_2O_4$ prepared through oxalates precursors. Polyhedron. 2011; 30: 1185–1190.

[20] Wang L, Li Z, Liang Y, et al. Characterization and electromagnetic properties of $Ni_{1-x}Cu_xFe_2O_4$ nanoparticle ferrites synthesized by using egg white. Adv Powder Technol. 2014; 25: 1510–1515.

[21] Patil DR, Chougule BK. Effect of copper substitution on electrical and magnetic properties of $NiFe_2O_4$ferrite. Mater Chem Phys. 2009; 117: 35–40.

[22] Fayek MK, Ata-Allah SS, Refai HS. On the cation distribution in $Ni_{1-x}Cu_xFe_{2-y}Al_yO_4$ spinel. J Appl Phys. 1999; 85: 325–328.

[23] Devan RS, Kolekar YD, Chougule BK. Effect of cobalt substitution on the properties of nickel–copper ferrite. J Phys: Condens Matter. 2006; 18: 9809–9821.

[24] Batoo KM, Ansari MS. Low temperature-fired Ni-Cu-Zn ferrite nanoparticles through auto-combustion method for multilayer chip inductor applications. Nanoscale Res Lett. 2012; 7: 112–125.

[25] Batoo KM, Abd El-sadek MS. Electrical and magnetic transport properties of Ni–Cu–Mg ferrite nanoparticles prepared by sol–gel method. J Alloys Compd. 2013; 566: 112–119.

[26] Tan X, Li G, Zhao Y, et al. The effect of Cu content on the structure of $Ni_{1-x}Cu_xFe_2O_4$ spinels. Mater Res Bull. 2009; 44: 2160–2168.

[27] Hoque SM, Choudhury MA, Islam MF. Characterization of Ni–Cu mixed spinel ferrite. J Magn Magn Mater. 2002; 251: 292–303.

[28] Anjum S, Rashid A, Bashir F, et al. Effect of Cu-Doped Nickel Ferrites on Structural, Magnetic, and Dielectric Properties. IEEE Trans Magn. 2014; 50: 2200504–2200507.

[29] Shannon RD. Revised effective ionic radii and systematic studies of interatomic distances in halides and chalcogenides. Acta Cryst. 1976; A32: 751–767.

[30] Dhahri A, Dhahri Ja, Hcini S, et al. Influence of Al substitution on physical properties of $Pr_{0.67}Sr_{0.33}Mn_{1-x}Al_xO_3$ manganites. Appl Phys A. 2015; 120: 247–253.

[31] Hcini S, Zemni S, Triki A, et al. Size mismatch, grain boundary and bandwidth effects on structural, magnetic and electrical properties of $Pr_{0.67}Ba_{0.33}MnO_3$ and $Pr_{0.67}Sr_{0.33}MnO_3$ perovskites. J Alloys Compd. 2011; 509: 1394–1400.

[32] Kiran HV, Shashimohan AL, Chakrabarty DK, et al. Structural and Magnetic Properties of Copper-Nickel Ferrites. Phys stat sol (a). 1981; 66: 743–747.

[33] Arrott A. Criterion for Ferromagnetism from Observations of Magnetic Isotherms. Phys. Rev. 1957; 108: 1394–1396.

[34] Banerjee SK. On a generalised approach to first and second order magnetic transitions Phys Lett. 1964; 12: 16–767.

[35] Franco V, Conde A, Romero-Enrique JM, et al. A universal curve for the magnetocaloric effect: an analysis based on scaling relations. J. Phys.: Condens. Matter. 2008; 20: 285207–285211.

Table 1: Magnetocaloric properties at a magnetic field $\mu_0 H = 5\ T$ of $Ni_{0.6}Cu_{0.4}Fe_{1.5}Cr_{0.5}O_4$ ferrite nanoparticle (present work) compared with several ferrites materials.

Composition	T_C (K)	ΔH (T)	$\lvert\Delta S_M^{max}\rvert$ ($J.K^{-1}.kg^{-1}$)	RCP ($J.kg^{-1}$)	Ref.
$Ni_{0.6}Cu_{0.4}Fe_{1.5}Cr_{0.5}O_4$	660	5	1.39	142	**PW**
$Zn_{0.6}Cu_{0.4}Fe_2O_4$	305	5	1.16	289	**[8]**
$Zn_{0.4}Ni_{0.2}Cu_{0.4}Fe_2O_4$	565	5	1.41	141	**[8]**
$Zn_{0.2}Ni_{0.4}Cu_{0.4}Fe_2O_4$	705	5	1.61	233	**[8]**
$Cu_{0.4}Zn_{0.6}Fe_2O_4$	373	5	1.77	-	**[10]**
$Cu_{0.2}Zn_{0.8}Fe_2O_4$	140	5	1.17	-	**[10]**

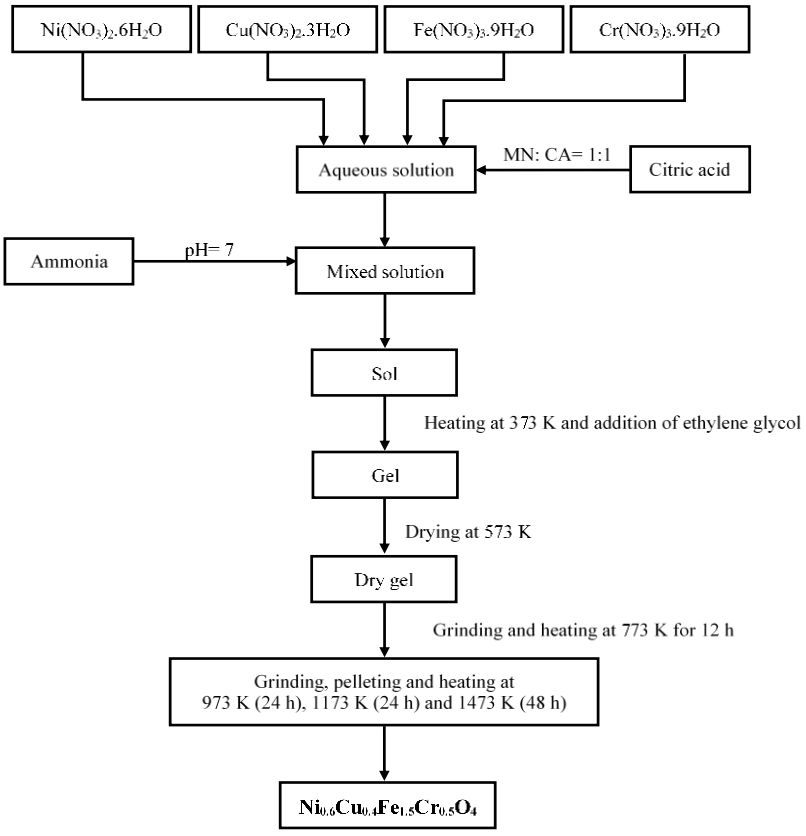

Figure 1: Schematic diagram representing the synthesis process of $Ni_{0.6}Cu_{0.4}Fe_{1.5}Cr_{0.5}O_4$ sample.

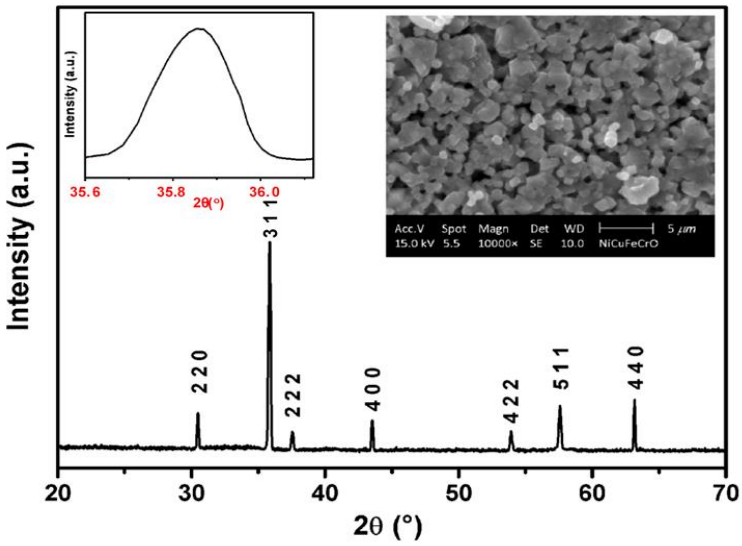

Figure 2: XRD pattern for $Ni_{0.6}Cu_{0.4}Fe_{1.5}Cr_{0.5}O_4$ sample. All peaks are indexed in the cubic spinel type structure with $Fd\bar{3}m$ space group. The left inset shows the most intense peak (3 1 1). The right inset the inset shows the SEM image.

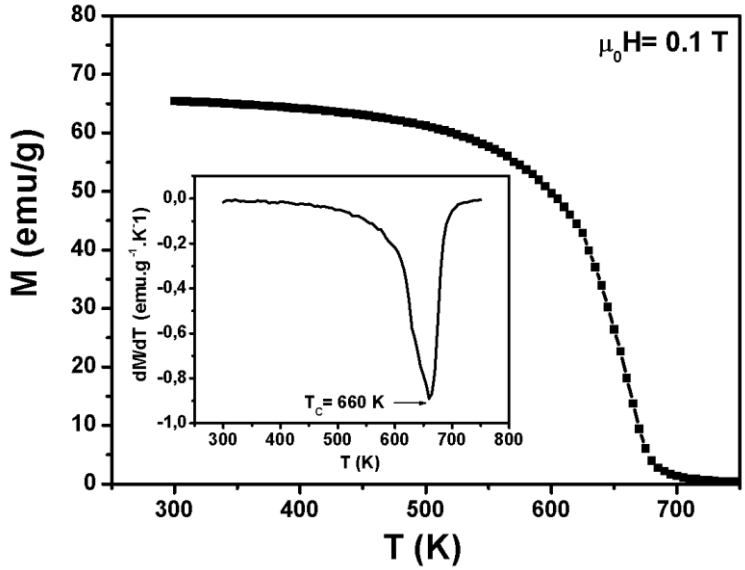

Figure 3: Magnetization as a function of temperature at applied magnetic field of 0.1 T measured for $Ni_{0.6}Cu_{0.4}Fe_{1.5}Cr_{0.5}O_4$ sample. The inset is the plot of *dM/dT* versus *T*.

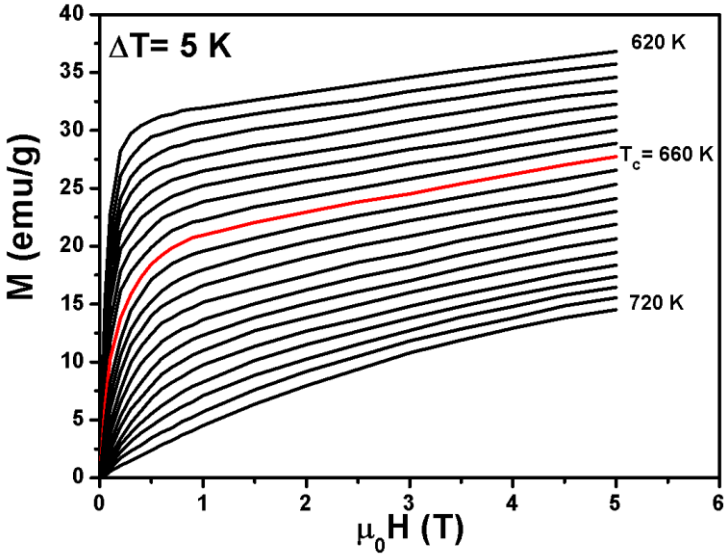

Figure 4: Isothermal magnetization $M(\mu_0 H, T)$ vs. applied magnetic fields, measured for different temperatures near T_C for $Ni_{0.6}Cu_{0.4}Fe_{1.5}Cr_{0.5}O_4$ sample.

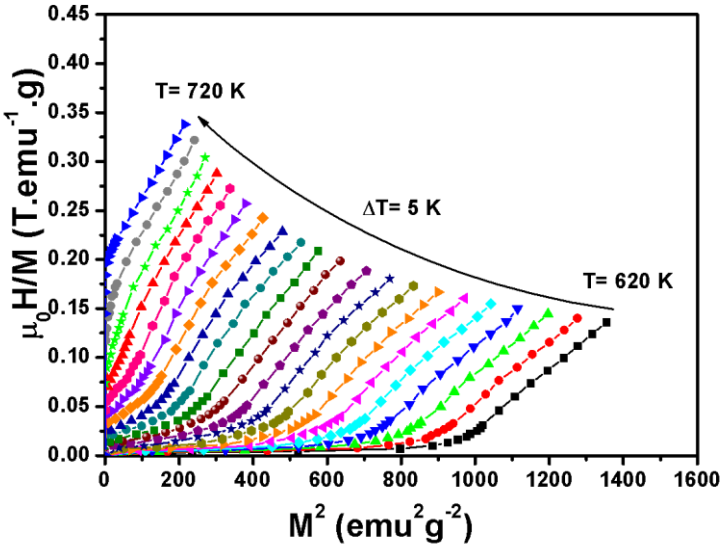

Figure 5: Arrott plots ($\mu_0 H/M$ vs. M^2) around T_C for $Ni_{0.6}Cu_{0.4}Fe_{1.5}Cr_{0.5}O_4$ sample.

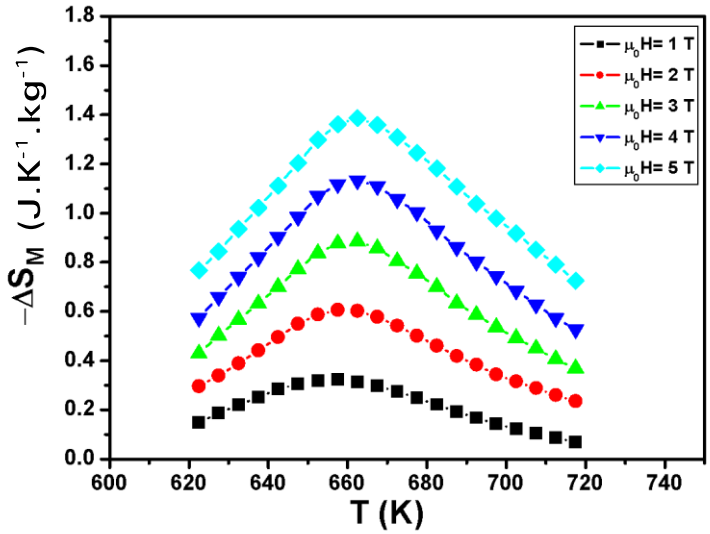

Figure 6: Temperature dependence of the magnetic entropy change at various applied magnetic fields for $Ni_{0.6}Cu_{0.4}Fe_{1.5}Cr_{0.5}O_4$ sample.

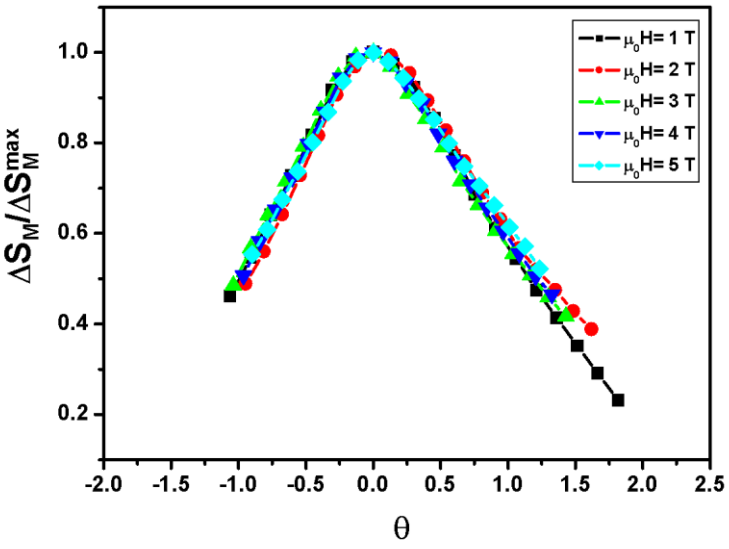

Figure 7: Normalized entropy change ($\Delta S_M/\Delta S_M^{max}$) as a function of the rescaled temperature (θ) for different applied magnetic fields for $Ni_{0.6}Cu_{0.4}Fe_{1.5}Cr_{0.5}O_4$ sample.

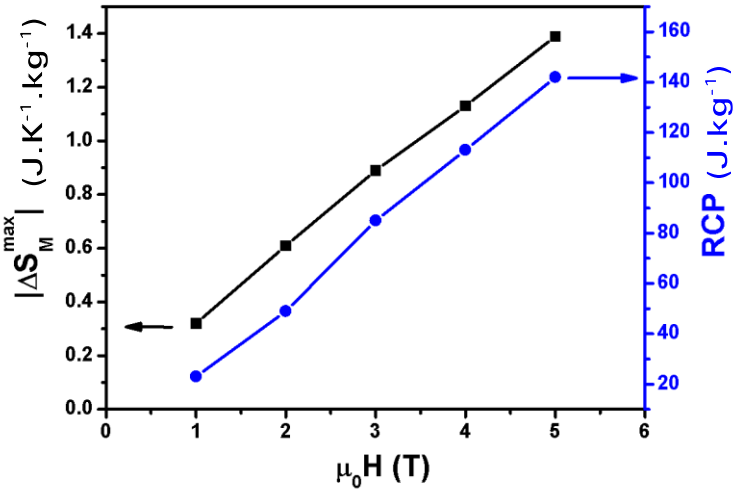

Figure 8: Maximum magnetic entropy change $|\Delta S_M^{max}|$ and relative cooling power values (RCP) vs. applied magnetic fields for $Ni_{0.6}Cu_{0.4}Fe_{1.5}Cr_{0.5}O_4$ sample.